Available online at www.sciencedirect.com
SCIENCE DIRECT®
International Journal of Heat and Fluid Flow 25 (2004) 288–297
International Journal of HEAT AND FLUID FLOW
www.elsevier.com/locate/ijhff

Bubble formation with pool boiling on tubes with or without basic surface modifications for enhancement

Dieter Gorenflo [a,*], Elisabeth Danger [a], Andrea Luke [a], Stephan Kotthoff [a], Untung Chandra [a], Chennu Ranganayakulu [b]

[a] *Wärme- und Kältetechnik, Universität Paderborn, Warburger Str. 100, D-33098 Paderborn 33098, Germany*
[b] *Aeronautical Development Agency, P.O. Box 1718, Bangalore, Karnataka 560017, India*

Abstract

Bubble formation is investigated on a single, horizontal copper tube ($D = 25.4$ mm) before and after applying surface modifications in the form of macrocavities with comparatively simple shapes (size: 200×100 μm on the tube surface and 50 μm in depth) in order to link bubble formation and heat transfer to the geometric features of the cavities. Two kinds of cavities exist in parallel, one with reduced mouth width (so-called "main structure") and one without this reduction ("secondary structure"). Pool boiling experiments with different organic liquids have been performed with variation of heat flux and saturation pressure. The resulting bubble formation on the tubes with and without surface modifications is discussed in terms of characteristic parameters such as local distribution and temporal activation behavior of the nucleation sites for bubble formation at active nucleation sites ("primary bubbles") or for bubbles released from the macrocavities ("secondary bubbles").

Keywords: Pool boiling; Heat transfer enhancement; Bubble formation

1. Introduction

Many efforts have been recently made to replace the existing, mainly empirical correlations for the heat flux from a heated wall to a pure liquid or mixture in pool boiling by a calculation method based on the (microscopic and macroscopic) events of vapor bubbles growing, departing and sliding on the wall, and with the interactions of neighboring bubbles. In this "search for a mechanistic [heat transfer] model" (Nelson et al., 1996), the activation and deactivation criteria for nucleation sites should be described which are the starting points of the whole heat transfer process. A review of the literature on interactions between heat transfer and bubble formation in nucleate boiling has been given in 1998 (Gorenflo et al., 1998) revealing that much less systematic investigations exist on bubble formation than on heat transfer, and that significant differences may occur between bubble formation on surfaces modified by macrostructures for enhancement of heat transfer and formation on surfaces of plain tubes with purely microscopic surface structures formed by their roughness.

In this paper, bubble formation is investigated on single, horizontal copper tubes with surface modifications in the frame of a joint DFG research project on fundamentals of nucleate boiling heat transfer. Experimental results are compared for the same test tube before and after applying surface modifications in the form of macrocavities with comparatively simple shapes in order to link bubble formation and heat transfer to the geometric features of the cavities. The sizes of the cavities are 200×100 μm on the tube surface and 50 μm in depth, and two kinds of cavities exist in parallel, one with reduced mouth width applied in an additional production step (so-called "main structure") and one without this reduction ("secondary structure"). Pool boiling experiments with different organic liquids have been performed with variation of heat flux and saturation pressure. The resulting bubble formation on the tubes with and without surface modifications is discussed in terms of characteristic parameters as local distribution and temporal activation behavior of the nucleation sites for bubble formation at active nucleation sites ("primary

* Corresponding author. Tel.: +49-5254-60-2393; fax: +49-5251-60-3522.
E-mail address: digo@wkt.uni-paderborn.de (D. Gorenflo).

0142-727X/$ - see front matter © 2003 Elsevier Inc. All rights reserved.
doi:10.1016/j.ijheatfluidflow.2003.11.018

bubbles'') or for bubbles released from the macrocavities (''secondary bubbles'').

2. Survey on characteristic heat transfer results

The design of the test tubes, the experimental procedure of the heat transfer measurements, and detailed heat transfer results have already been published elsewhere (cf. e.g. Gorenflo et al., 2000a,b, 2002a,b; Danger et al., 2001). For comparison with bubble formation, some of the characteristic heat transfer features are briefly discussed here.

In the double logarithmic diagram of the heat transfer coefficient α versus heat flux q at the top of Fig. 1, a typical run at constant pressure p_s equal to 10% of the critical pressure p_c of propane is given for the fine sandblasted tube surface (mean roughness $P_a = 0.25$ μm) *before* applying surface modifications. The heat fluxes range from fully developed nucleate boiling at $q = 70$ kW/m^2 down to 0.1 kW/m^2 at natural convection without bubble formation. The circumferential distribution of the superheat $\Delta T = T_W - T_s$ of the tube surface at an intermediate heat flux within the nucleate boiling domain (solid square at $q = 19.96$ kW/m^2 in the upper diagram) is represented in the lower diagram for the two cross sections equipped with thermocouples within the regions of the main (big squares) and secondary (small squares) structure. As can be seen, the distributions (before applying surface modifications) agree quite well, with their integrated mean values differing by less than 0.5%, although the two cross sections are separated 30 mm from each other in axial direction of the tube. The overall heat transfer coefficients for the tube without surface modifications are always calculated by

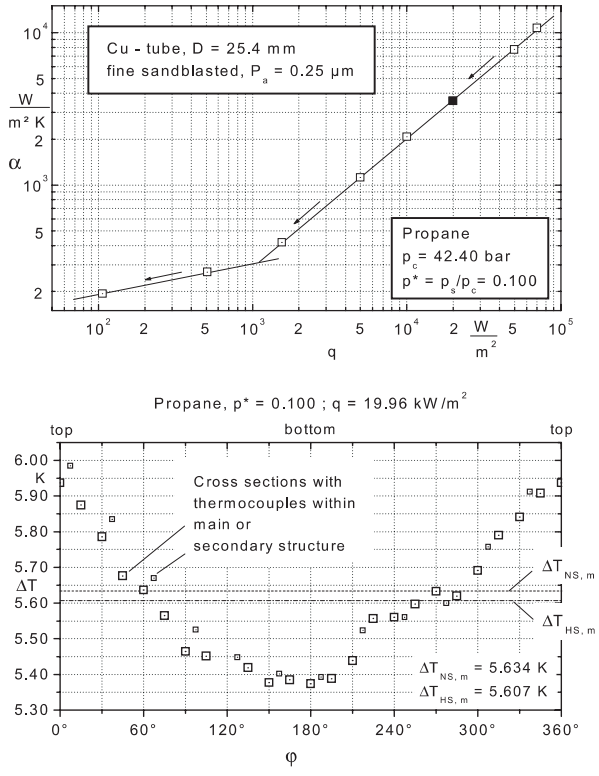

Fig. 1. Typical run of the heat transfer measurements at constant pressure for propane boiling on the fine sandblasted Cu tube without surface modifications (top) and superheat ΔT as function of the azimuthal angle φ for two cross sections within the regions of the main and secondary structure (bottom) at the heat flux indicated by solid symbol in the upper diagram.

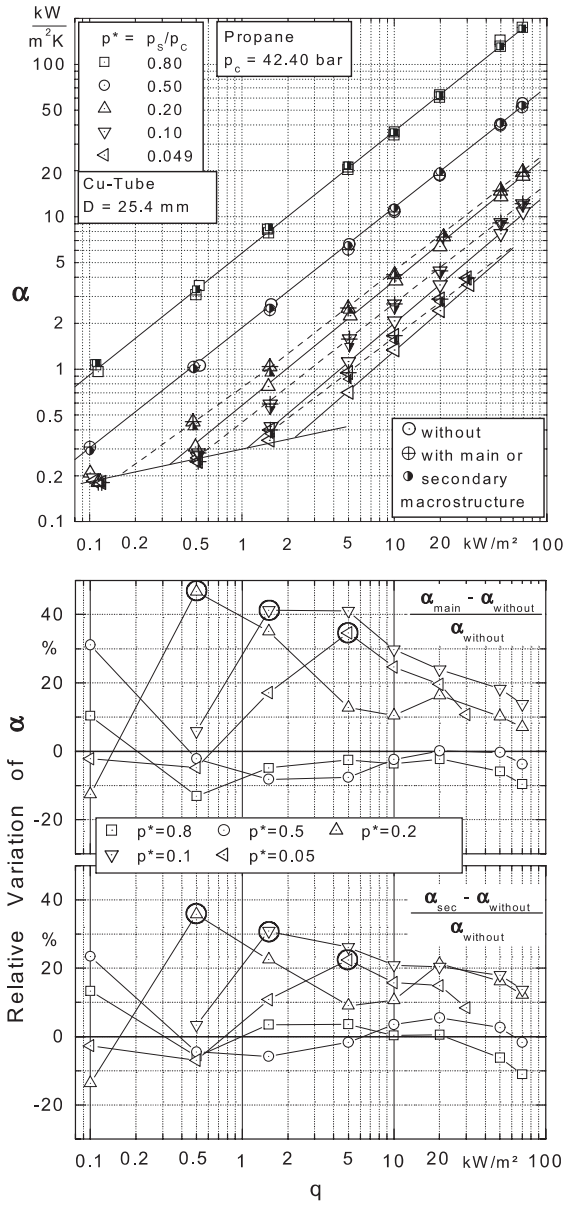

Fig. 2. Heat transfer from a horizontal Cu tube with or without surface modifications to propane at different heat fluxes and normalized pressures (top) and relative variation of α by the surface modifications in per cent (bottom) (from Gorenflo et al. (2002b)).

$$\alpha = q/\Delta T = (Q/A)/(T_W - T_s), \quad (1)$$

where Q is the electrical energy input to the tube heater, A is the heated part of tube surface, and ΔT is the integrated mean value of the superheat for *both* cross sections, measured directly by the thermocouples in the tube wall and their reference junctions in the pool of boiling liquid below the tube, with the temperature drop from the location of the thermocouples to T_W of the tube surface being taken into account by assuming purely radial heat conduction within the tube wall.

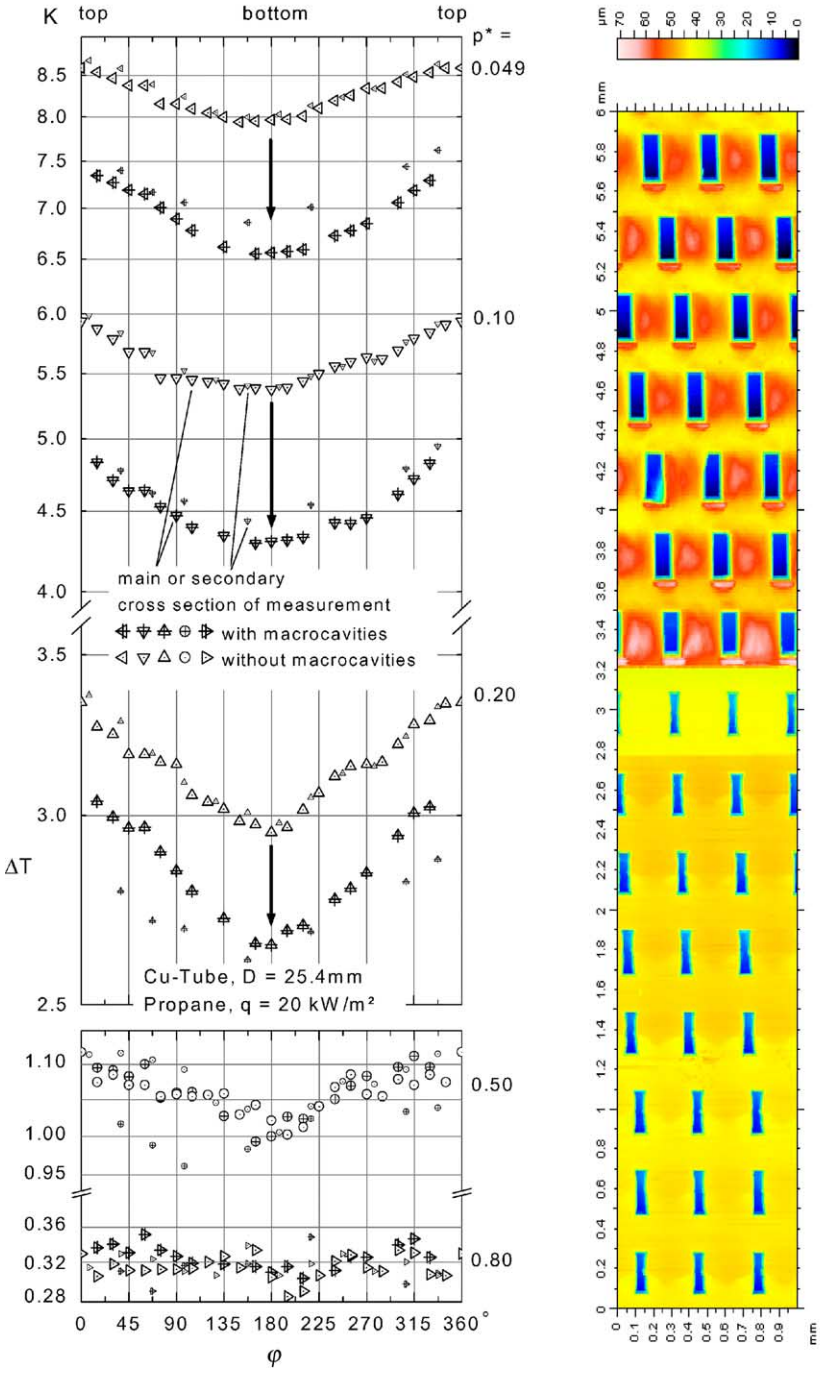

Fig. 3. Variation of the local wall superheat ΔT with the azimuthal angle φ for different normalized pressures p^* at constant heat flux $q = 20$ kW/m^2 (left) and topography of the surface structures on the copper tube (near the border line between the two different structures at 3.2 mm) in a representation with the depths of the cavities indicated by different gray levels starting at the base lines of the macrocavities (right; notice the 'heights' of approx. 60 µm between the cavities of the secondary structure) (from Gorenflo et al. (2002b)). Largest dimension of the cavities in the direction of the tube axis. Main structure: bottom; secondary structure: top.

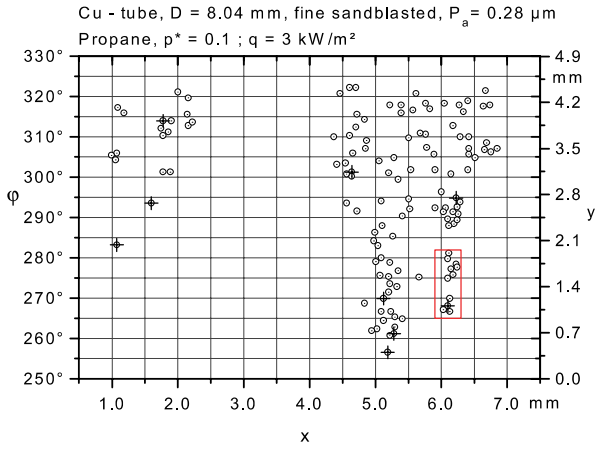

Fig. 4. Local distribution of active nucleation sites on the flank of a horizontal copper tube for propane boiling at $p^* = 0.1$ and $q = 3$ kW/m^2.

In Fig. 2 the overall heat transfer coefficients with and without surface modifications are shown for the measurements with propane at different normalized saturation pressures p^*. Comparing the open with the corresponding modified symbols or the solid with the dashed interpolation lines, it can be seen that α increases significantly as a result of the surface modifications, particularly at small heat fluxes near the onset of nucleation and at intermediate normalized saturation pressures between 5% and 20% of the critical pressure, but not at normalized pressures greater than approximately $p^* = 0.5$.

The relative variation of α caused by the macrostructures is given in the lower diagrams for the main (top) and secondary (bottom) structures. The higher heat transfer enhancement caused by the main structure and the common trend of decreasing enhancement

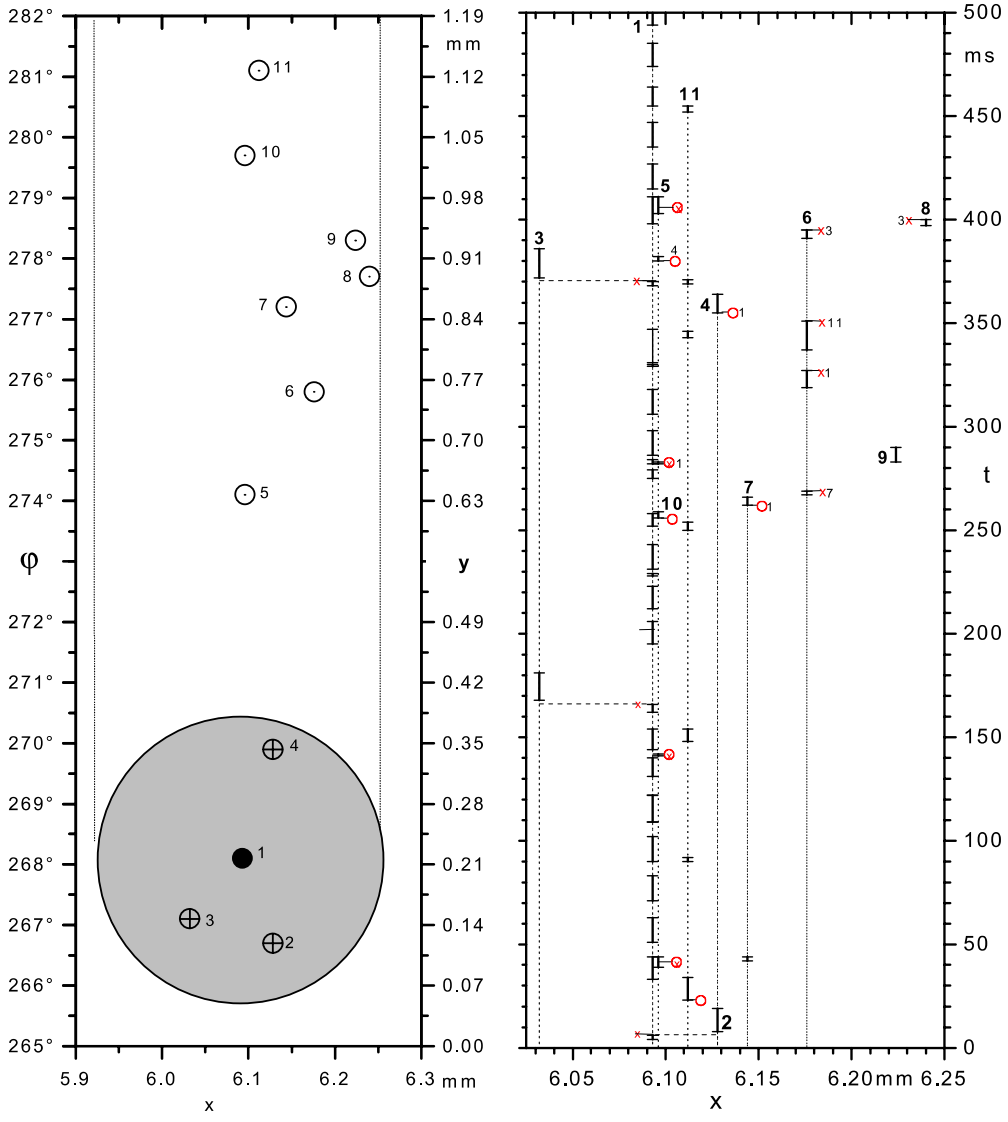

Fig. 5. Local distribution of the 11 active sites within the marked rectangle in Fig. 4 (left) and mean bubble departure diameter for site #1 (grey, to scale), and time history of bubble production during the video sequence of 500 ms (right).

towards high normalized pressures and heat fluxes is quantified here in detail. As can be seen the best heat transfer enhancement is connected to a certain low to intermediate heat flux range and corresponding low to intermediate active site density near beginning nucleation, and as a consequence, the maximum relative increase of α shifts to higher heat fluxes for lower normalized pressures (compare the three symbols in circles in each of the two lower diagrams of Fig. 2), because site activation decreases with decreasing pressure.

The variation of the local wall superheat ΔT with the azimuthal angle φ and the normalized pressure p^* is represented in Fig. 3 (left) for propane boiling at constant intermediate heat flux $q = 20$ kW/m^2. While at the highest pressure no influence of the azimuthal position on the local superheat is observed, there is a significant enhancement of heat transfer on the lower parts of the tube surface at intermediate normalized pressures with a maximum at $p^* = 0.10$. This holds for the measurements without surface modifications (open symbols) and also with surface modifications (modified symbols).

It is likely that the enhancement below the flank of the tube results from the prolonged contact of the bubbles with the thin superheated liquid layer in the immediate vicinity of the tube wall—either at the nucleation site itself (bottom) or when sliding upwards—due to the component of the buoyancy force directed towards the tube surface. Above the flank, this effect vanishes, because the rising bubbles gradually lose contact with the whole superheated liquid layer and furthermore, the superheated liquid layer—accelerated by sliding bubbles and augmenting near the tube surface in the upper parts—is caught by vortex effects at the top of the tube, thus increasing the thickness of the layer and the heat transfer resistance.

This combined convective and evaporative enhancement of heat transfer by the sliding bubbles is strongest when the number of bubbles is neither too small nor too high, i.e. at (low to) intermediate densities of active nucleation sites on the heated surface. That is why it loses importance towards low or high *normalized* pressures (or very low or very high heat fluxes, cf. Gorenflo et al., 2000a; Danger et al., 2001), because site activation is reduced with decreasing pressure at constant heat flux in a similar way as with decreasing heat flux at constant pressure.

The surface structures on the copper tube near the border line between the main (0–3 mm) and secondary (3.2–6 mm) structures are demonstrated by the topographies in Fig. 3 on the right. The sections show approximately 1×3 mm in a representation where the depths of the macrocavities are indicated by different gray levels. The cavities of the simpler secondary structure are purely radially orientated in depth (size: approx. $200 \times 100 \times 50$ μm), and the cavities of the main structure are modified in order to produce reentrant effects. The microstructure of the surface roughness on the areas between the macrocavities *of the main structure* has been flattened severely during the second step of the surface modification (a rolling process).

3. Typical example for the analysis of bubble formation

Data taken from the flank of a horizontal copper tube with 8.04 mm diameter and fine sandblasted surface ($P_a = 0.28$ μm) are used in Figs. 4–6 as typical example for the analysis of bubble formation *without macrocavities* on the tube surface. In Fig. 4 the local distribution of active nucleation sites—approached with decreasing heat flux—is shown for propane boiling at $p^* = 0.1$ and

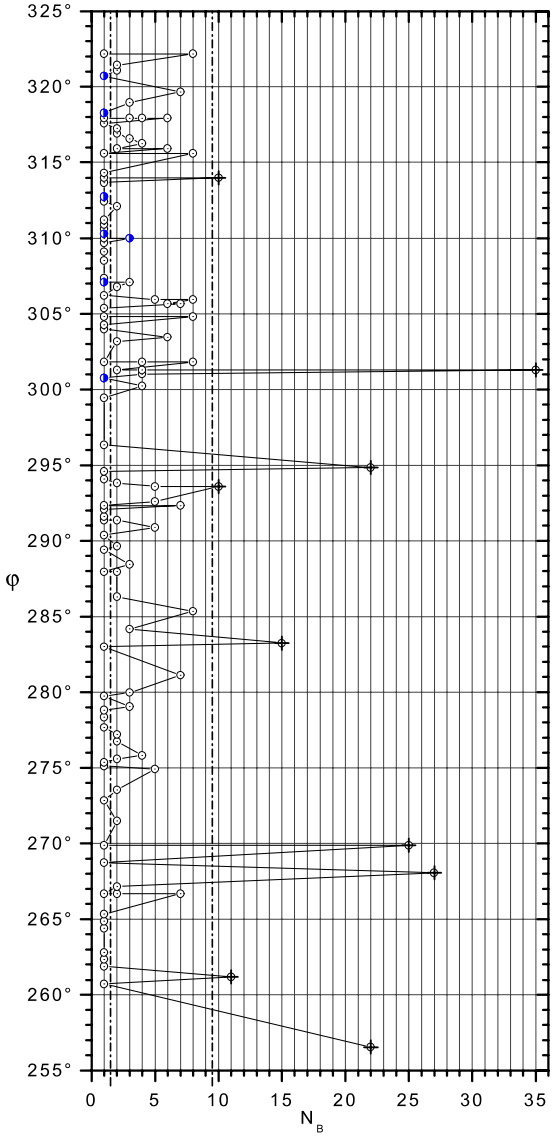

Fig. 6. Number N_B of bubbles originating from each of the active sites of Fig. 4 during 500 ms.

Table 1
Summarized analysis of the video frames containing the active cavities #1 to 11 of Fig. 5

Active cavities, #		1	2	3	4	5	6	7	8	9	10	11
Position: X [mm]		6.093	6.128	6.032	6.128	6.096	6.176	6.144	6.240	6.224	6.096	6.112
Y [deg]		267.1	266.7	267.1	269.9	274.1	275.8	277.2	277.7	278.3	279.7	281.1
Cycles of bubble formation [500 ms^{-1}]		27	1	2	1	5	4	2	1	1	1	7[a]
Growing period [ms]	max	17	–	15	–	9	15	5	–	–	–	12
	mean	10	12	15	10	4	8	4	4	8	4	5[a]
	min	2[b]	–	14	–	2	3	3	–	–	–	3
Waiting period [ms]	max	28	–	–	–	139	49	–	–	–	–	95
	mean	10	–	191	–	89	33	218	–	–	–	59
	min	0[b]	–	–	–	20	9	–	–	–	–	22
Activated[c]		–	–	–	1	5	–	1	–	–	1	1[a]
Detached[c]		3	–	–	–	4	4	–	1	–	–	–[a]
d_a [mm][d]	mean	0.334	0.341	0.389	0.330	0.160	–	0.213	–	0.288	–	0.275
w [mm/s][d]	mean	36.7	40.7	43.1	36.8	–	–	32[e]	–	–	–	–

Cu tube, $D = 8.04$ mm, fine sandblasted, $P_a = 0.28$ μm; propane, $p^* = 0.1$, $q = 3$ kW/m^2; o(No.) or x(No.) = activated or detached, respectively, by a sliding bubble from site (No.).

[a] Short mean growing period, although six out of seven bubbles without hydrodynamic interaction with other bubbles.

[b] Growing periods could be shorter and waiting periods longer, both almost up to 2 ms, because the picture is exposed for 80–90% of the entire time interval of 1 ms per frame.

[c] Activated or detached by interaction with other bubbles.

[d] d_a = departure diameter (without direct interaction with other bubbles); w = rising velocity (up to 5 mm after detachment).

[e] The remaining bubbles from cavities #5 to 11 were covered or severely influenced by other bubbles immediately after detachment, so their rising velocity could not be determined.

$q = 3$ kW/m^2, and the 11 cavities within the rectangle at $x = 6$ mm, $y = 1.4$ mm have been enlarged in Fig. 5. As can be seen on the left of Fig. 5, the nucleation sites #2 to 4 lie within the (projected) mean departure diameter of the bubbles originating from the very frequently active site #1 (27 times active during 500 ms, see on the right) or along their way up on the tube surface.

On the right hand side, the growing period of each bubble has been indicated by a bar, and the circles or crosses mean that activation or detachment, respectively, were initiated by another bubble. For instance, the only bubble originating at site #4 was activated by a bubble from site #1, and the bubble at site #8 was detached by a bubble from site #3. The whole bubble formation history at the 11 active sites is summarized in Table 1.

The data reveal that the growing periods at the same active site differ markedly between the maximum and minimum value, and the mean values for sites #5 to 11 are significantly shorter and the departure diameters d_a smaller than for sites #1–4, indicating the influence of the frequently active site #1 (so-called "stable" site). The same holds for the activation of sites above the eight other frequently active sites indicated by crosses in Fig. 4, and together with site #1, the nine stable sites appear again in Fig. 6, where the number N_B of bubbles originating from each of the active sites of Fig. 4 during a video sequence of 500 ms is related to the azimuthal position φ of the site. As can be seen, 10 or more bubbles are produced at each of the nine stable sites during 500 ms, while slightly less than 50% of all active sites are only active once within the whole sequence, and the production rates for the remaining 50% lie in between.

When analyzing the video sequences, the number of active sites per surface area of the heated tube (= site density) is important under two aspects: On the one hand, the number N_{sim} of sites *simultaneously active* should be known to estimate the part of the entire heat input that is used for vapor production, and on the other hand the number N_{cum} of all of those sites should be known that are active at least once during a longer time period (= cumulative site density) to connect N_{cum} to the

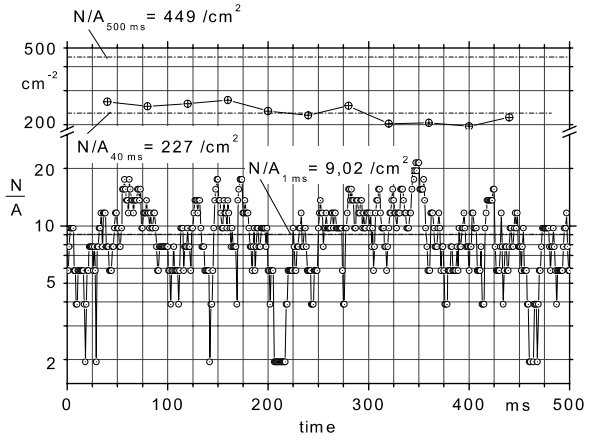

Fig. 7. Number $(N/A)_{sim,1\,ms}$ of simultaneously active sites (time period: 1 ms; bottom) and pertaining cumulative values for 40 or 500 ms (above). Example: R134a at $p^* = 0.1$ and $q = 10$ kW/m^2 on the fine sandblasted Cu tube ($D = 25.4$ mm; $P_a = 0.25$ μm).

microstructure of the heated surface (= potential site density) and to derive activation criteria.

In Fig. 7 the number $(N/A)_{\mathrm{sim,1ms}}$ of simultaneously active sites for each video frame (1 ms) is represented at the bottom, and the pertaining cumulative values for 40 or 500 ms, respectively, are given above. As can be seen, the number of simultaneously active sites varies tremendously, almost by ±100% of the mean value $(N/A)_{\mathrm{sim}} = 9.02/\mathrm{cm}^2$. The following mechanism could explain this oscillating behavior: When only a few bubbles are produced, the constant electrical heat input may be higher than the heat removed, resulting in rising wall superheat. This in turn will activate so many bubbles that more heat is removed than added, and the superheat decreases again below the equilibrium value. The same behavior occurs *with macrocavities* (see Fig. 12).

Increasing the time period by a factor of 40 (to 40 ms), the mean value of N/A rises by a factor of approx. 25 (to 227/cm^2) and the scatter is reduced to ±20%, while a further increase of the period by a factor of 12 (to 500 ms) results roughly in the double number of active sites (449/cm^2), which will be close to the overall number of cavities within the microstructure of the surface that can ever be activated under the steady state conditions of this example. The evaluation is consistent with results of Barthau and Hahne (2001) for a gold-plated copper tube with the same surface treatment.

An abbreviated representation for the evaluation of cumulative and simultaneously active sites as discussed in Figs. 4–6 in detail is given in Fig. 8 for the significantly higher heat flux $q = 20$ kW/m^2. This representation also demonstrates that there are many similar neighboring cavities within the homogeneous surface structure of the 25.4 mm Cu tube which could remove

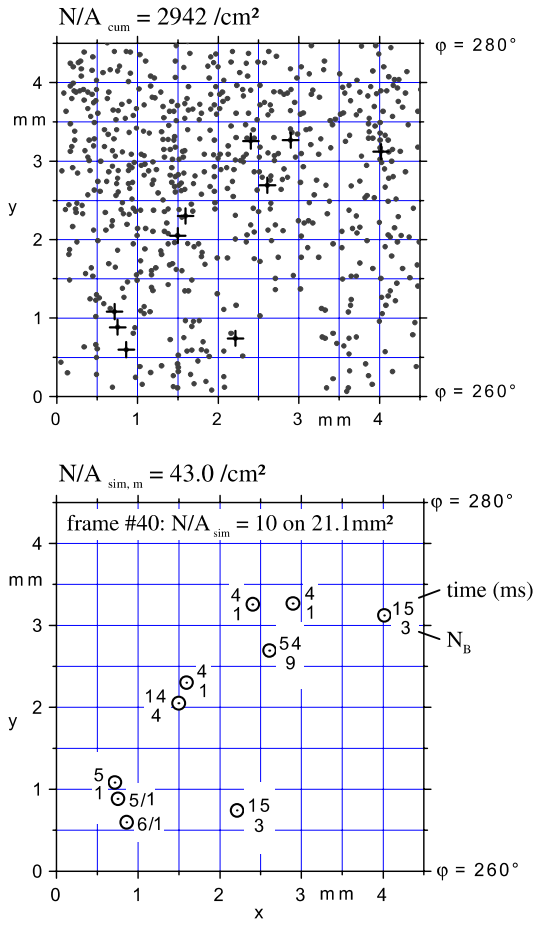

Fig. 8. Local distribution of active sites for propane ($p^* = 0.1$ and $q = 20$ kW/m^2) near the flank of the fine sandblasted Cu tube ($D = 25.4$ mm; $P_a = 0.25$ μm). Top: Cumulative number for 500 ms; Bottom: Simultaneously active sites (1 ms). Numbers indicate the activation period (ms) and the number N_B of bubble formation cycles, both per active site and 500 ms.

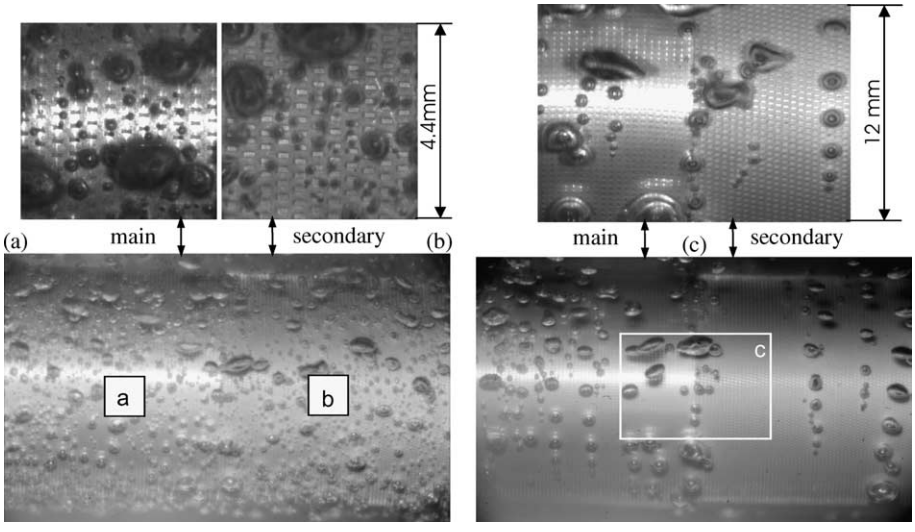

Fig. 9. Bubble formation near the border line between the main and secondary structures at $p^* = 0.1$, $q = 10$ kW/m^2 (a,b) and at $p^* = 0.049$, $q = 5$ kW/m^2 (c). Lower pictures showing the entire diameter of 25.4 mm of the tube taken by a photo camera, upper details extracted from digital high-speed video sequences (1000 frames per second). Main structure always on the left.

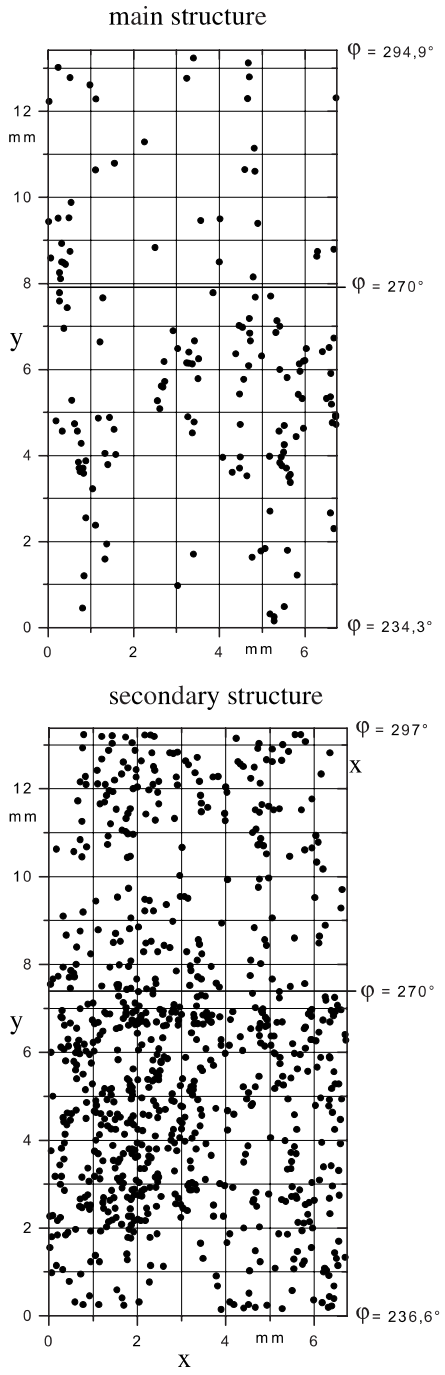

Fig. 10. Local distribution of cumulative number of active sites during 500 ms on the main (top) or secondary (bottom) structure, resp., of the 25.4 mm Cu tube near the flank ($\varphi = 270°$). Example: 2-propanol, $p^* = 0.10$, $q = 10$ kW/m^2.

the electrical heat input (ca. factor of 70 between cumulative and simultaneously active number of sites; see also Fig. 11). On the other hand, the analysis in the lower diagram reveals that the temporal activation behavior of each individual site is very similar to the example of Figs. 4–6 with much smaller overall heat flux.

4. Bubble formation on the modified surfaces

Fig. 9 shall give a direct impression of bubble formation on the modified surfaces at low to intermediate heat fluxes and normalized pressures where heat transfer enhancement by the surface modifications and the combined convective and evaporative effects of the sliding bubbles on the enhancement is greatest, as follows from Figs. 2 and 3. The lower pictures for each of the two boiling conditions were taken by a photo camera, and the details above were extracted from digital high-speed video sequences taken at 1000 frames per second with higher magnifications (size of the areas indicated by a–c).

As can be seen, the bubble dimensions are quite different within each of the two pressures shown: there are very small bubbles leaving their sites and others with much larger diameters coming from the lower parts of the tube. Their bigger sizes may result from

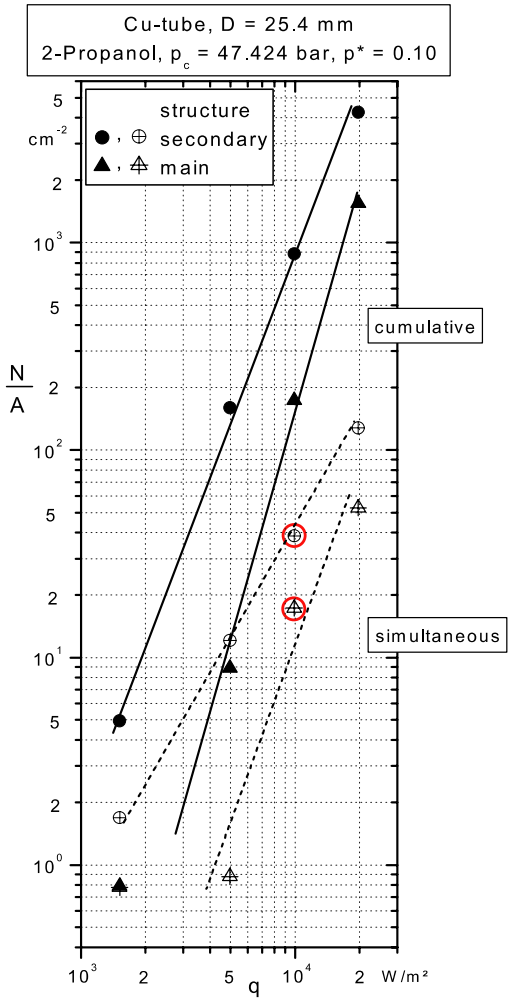

Fig. 11. Cumulative (closed symbols) and simultaneous (open symbols) site density N/A on the main or secondary structure, resp., for 2-propanol boiling at constant normalized pressure $p^* = 0.10$ and various heat fluxes q.

- longer growing periods of the bubbles due to the component of the buoyancy force perpendicular to the tube surface,
- absorbing part of the superheated boundary layer while sliding along the tube surface and
- merging with other bubbles on their way up.

These effects can also be observed on tube surfaces without macrostructures.

Significant differences of the overall bubble production on the two structures and of the activation behavior of the macrocavities follow from Figs. 10–13: The cumulative number of active sites is much larger on the secondary structure than on the main (Figs. 10 and 11), and the same holds for the simultaneously active sites (Figs. 11 and 12), and this if *all* sites are taken into account or the active *macrocavities* only (Fig. 12). This

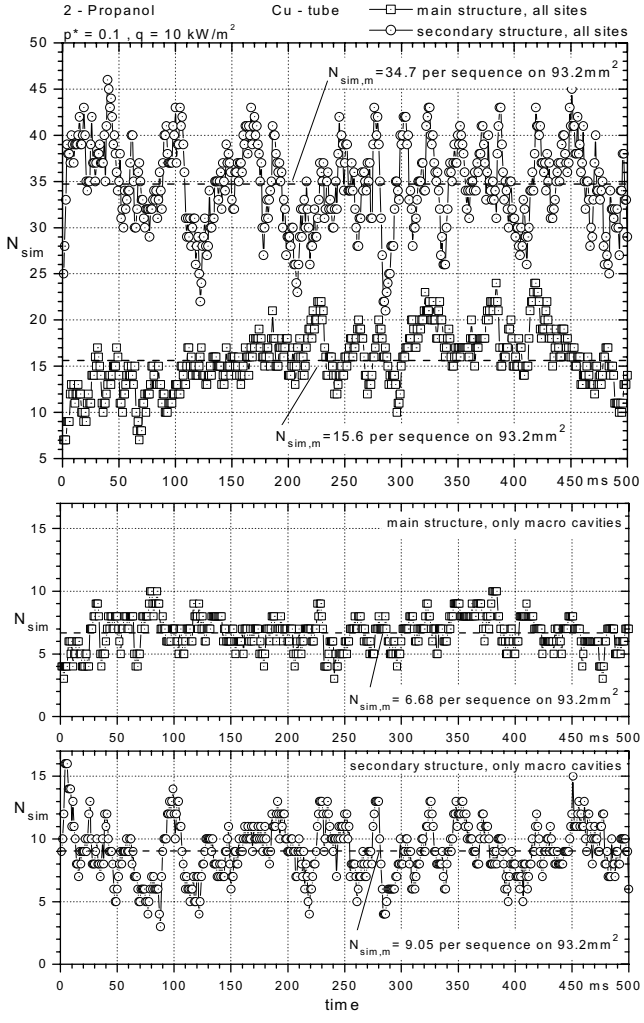

Fig. 12. Number N_{sim} of simultaneously (1 ms) active sites at $q = 10$ kW/m^2 (symbols in circles in Fig. 11) on the main or secondary structure, resp., during 500 ms. Upper diagram: all active sites; Two lower diagrams: active macrocavities only.

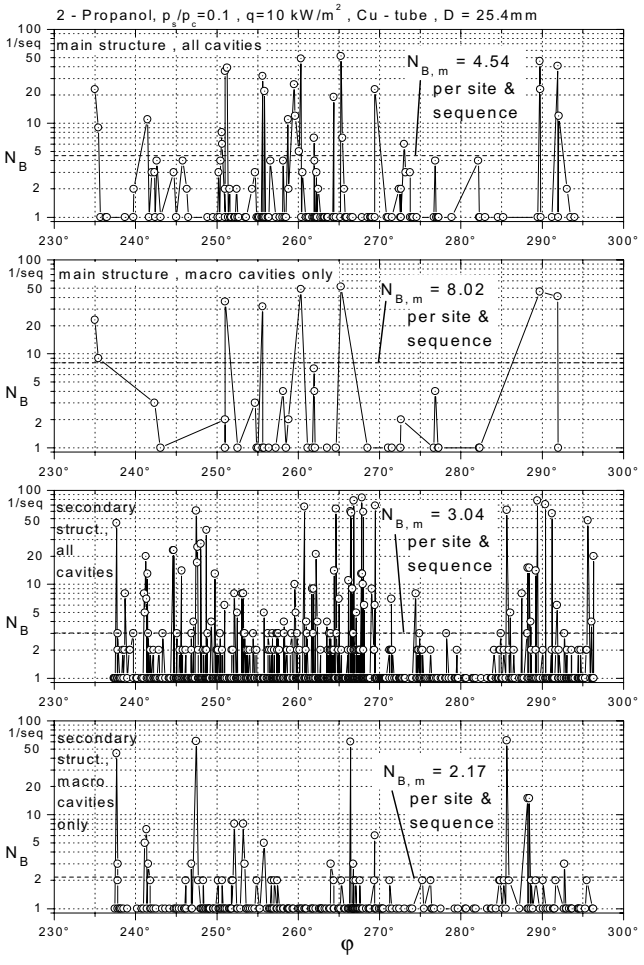

Fig. 13. Azimuthal distribution of active sites and number N_B of bubbles originating from each site for the same conditions as in Fig. 12. Diagrams at the top: main structure, at the bottom: secondary structure.

shows that the macrocavities of the main structure with their reentrant characteristics are more 'effective' than those of the secondary structure, which produce less (or similar, respectively) heat transfer enhancement despite their greater number N_{sim} (cf. Fig. 2).

The higher 'effectivity' of the macrocavities on the main structure is demonstrated by the higher number N_B of bubbles produced per site (so-called stable sites) than on the secondary (Fig. 13), this compensating the smaller number of simultaneously active sites when the same heat flux q exists on the tube surface within each of the two structures. Comparing the date for *all* cavities in Fig. 13 with those for the macrocavities only, reveals that the activation behavior of the macrocavities with their comparatively simple shape on the secondary structure obviously differs much less from that of the cavities produced by the surface roughness than in the case of the macrocavities on the main structure. In this comparison, however, it has to be taken into account that the original roughness of the sandblasted tube

surface *between* the macrocavities has been flattened severely during the second treatment of the tube (which produced the reentrant effects), and that therefore this part of the surface is much less active in bubble production in the case of the main than of the secondary structure.

As already these first analyses show in combination with the heat transfer results of Figs. 2 and 3, it is obvious that similar (or only slightly different) heat transfer enhancement can follow from significantly different activation history of the sites—compare $N_{sim,m}$ and $N_{B,m}$ for the two structures—and that the activation history may contain tremendous differences of simultaneous bubble production—compare the huge deviations of N_{sim} or N_B from their average values $N_{sim,m}$ or $N_{B,m}$, respectively. For further insight, more video sequences have to be analyzed, and especially the evaluation of bubble departure diameters and additional evaporation in sliding bubbles is missing till now to complete the present investigation.

For instance, this will certainly reveal that the average size for the 'secondary' bubbles leaving the macrocavities will be greater than for the ('primary') bubbles originating from the cavities within the roughness structure of the tube surface.

Acknowledgements

The authors appreciate financial support of Deutsche Forschungsgemeinschaft (DFG) in the frame of a joint research project on fundamentals of boiling heat transfer. Thanks are due to Fa. Wieland AG Ulm (Germany) for producing the modified tube surfaces.

References

Barthau, G., Hahne, E., 2001. Nucleate pool boiling of R134a on gold-plated copper test tube. Proc. Int. Inst. Refrig. Comm. B1 Conf. 2001/5, Paderborn, paper III. 25, pp. 372–379.

Danger, E., Chandra, U., Gorenflo, D., Beutler, A., 2001. Basic modifications of the heated surface for enhancement of pool boiling heat transfer. Proc. Int. Inst. Refrig. Comm. B1 Conf. 2001/5, Paderborn, paper III. 26, pp. 380–387.

Gorenflo, D., Luke, A., Danger, E., 1998. Interactions between heat transfer and bubble formation in nucleate boiling. In: Lee, J.S. (Ed.), Heat Transfer 1998, vol. 1. Taylor & Francis, Levittown, pp. 149–174.

Gorenflo, D., Fust, W., Luke, A., Danger, E., Chandra, U., 2000a. Pool boiling heat transfer from tubes with basic surface modifications for enhancement—design of the test tubes and first measurements. Proc. Third European Thermal Sciences Conf., vol. 2, pp. 743–748.

Gorenflo, D., Hübner, P., Fust, W., Luke, A., Danger, E., Chandra, U., 2000b. Pool boiling heat transfer and bubble formation of natural refrigerants on horizontal tubes. Proc. Fourth Gustav Lorentzen Conf., Int. Inst. Refrig. Comm. B1, B2, E1 and E2, pp. 419–427.

Gorenflo, D., Chandra, U., Danger, E., Luke, A., 2002a. Pool boiling heat transfer from tubes with and without basic surface modification for enhancement. Proc 12th Int. Heat Transfer Conf., vol. 3, pp. 521–526.

Gorenflo, D., Luke, A., Danger, E., Chandra, U., Kotthoff, S., 2002b. Heat transfer and bubble formation of Propane boiling on tubes with basic surface modifications for enhancement. Proc. Fifth Gustav Lorentzen Conf., Int. Inst. Refrig., pp. 363–370.

Nelson, R., Kenning, D., Shoji, M., 1996. Nonlinear dynamics in boiling phenomena. J. Heat Transf. Soc. Jpn. 35 (136), 22–34.